www.adeepakpublishing.com

Dickmann, S. R. et al. (2020): JoSS, Vol. 9, No. 3, pp. 921–935
(Peer-reviewed article available at www.jossonline.com)

www. JoSSonline.com

Automated Periapsis Time Estimation for the Aerodynamic Deorbit Experiment

Samantha R. Dickmann and David A. Spencer

Purdue University
West Lafayette, IN US

Brandon A. Smail

Northrop Grumman
Promontory, UT US

Abstract

Periapsis time estimation may be used to schedule on-orbit activities in an automated fashion. Previous applications of periapsis time estimation include aerobraking sequence timing adjustments for Mars orbiter missions. The Aerodynamic Deorbit Experiment (ADE) CubeSat will apply an algorithm for periapsis time estimation to autonomously schedule inertial measurement unit data acquisition during low-altitude atmospheric drag passes in Earth orbit. Following deployment of a drag sail, ADE will deorbit from an initial geosynchronous transfer orbit. During each drag pass, centroiding and integration of the measured acceleration profile are used to determine estimates of the periapsis time and the change in velocity, respectively. The orbital period is then updated, and the time of the subsequent periapsis is predicted. Simulation and analysis of the periapsis time estimation performance shows that the algorithm can predict periapsis times with an average error of 60 seconds and 1-sigma deviation of 20 seconds, based upon the root-sum square of individual error sources. This level of accuracy in the periapsis time estimation is sufficient to meet the measurement objectives for the Aerodynamic Deorbit Experiment.

1. Introduction

A periapsis time estimation (PTE) algorithm may be used for autonomously predicting future periapsis times based upon acceleration data collected during previous periapsis passes. For an orbital mission with periapsis within the sensible atmosphere, PTE can be useful for adjusting on-board sequence timing. Previously, PTE algorithms have been developed for aerobraking applications at Mars (Johnson, 2003; Spencer, 2007; Denis, 2018). Aerobraking missions including Mars Odyssey, Mars Reconnaissance Orbiter (MRO), Mars Atmosphere and Volatile Evolution Mission (MAVEN), and ExoMars have each utilized some aspect of PTE to enact sequence timing adjustments.

PTE was initially developed for Mars orbiter projects by Lockheed Martin. The algorithm was devel-

Corresponding Author: Samantha R. Dickmann – sdickma@purdue.edu
Publication History: Submitted – 9/14/19; Accepted – 8/28/20; Published: 9/30/20

Copyright © A. Deepak Publishing. All rights reserved.

oped and validated using atmospheric drag pass accelerometer data gathered from the Mars Global Surveyor (MGS). This first iteration was based on a periapsis timetable, a list of the predicted times of future periapsis passes, which could be updated via ground command. The PTE used a centroiding scheme to calculate the "time-center" of an acceleration curve gathered during a drag pass. The difference between this measured drag pass centroid and the prior predicted periapsis time was then used to provide adjustments to the subsequent periapsis time predictions, and the associated timing of the sequenced aerobraking activities. This method of PTE suffered from significant errors in large-period orbits greater than six hours, but for short-period orbits, the predicted periapsis times matched navigation reconstructions well, generally to within 30 seconds (Johnson, 2003). Lockheed Martin's PTE was improved upon and applied to Mars Odyssey and MRO aerobraking, as well as the MAVEN "deep dive" campaigns (Jesick, 2016). For these missions, the spacecraft's orbit period was calculated from the time between two consecutive time-centers. Acceleration data was used to estimate the change in velocity from each drag pass. These values were used to improve the accuracy of the upcoming periapsis time estimation.

The PTE algorithm serves as the cornerstone of autonomous aerobraking capability. Aerobraking maneuvers require precise timing for sequences to successfully execute. For aerobraking missions without an onboard periapsis time estimation process, periapsis times were calculated on the ground and uplinked to the spacecraft as a file. However, due to orbit-to-orbit density variations, these estimations would quickly become inaccurate (Johnson, 2003). For missions with periapsis timing requirements but limited communication windows, such as MAVEN, PTEs offer self-updating time estimations that do not rely on constant maintenance from the ground (Jesick, 2016). Therefore, PTEs are crucial for autonomously performing time-sensitive aerobraking sequences in situations with limited uplink and downlink or varying atmospheres.

Discussion of PTE in the literature centers on its use on Mars aerobraking missions for autonomous operations and for recreating atmospheric profiles (Lyons, 2001; Chapel, 2005; Tolson, 2011). Others focus on how accelerometer data must be processed and note that recent advancements in IMU technology may enable the use of simpler PTEs such as this one on missions (Jah, 2001; Jah, 2008; Hanna, 2002). Current research on the topic of autonomous aerobraking includes the development of more complex software involving PTE-like algorithms along with other sensors and algorithms for more accurate and more autonomous aerobraking (Prince, 2012; Carrelli, 2012).

In this work, the mathematical approach for PTE and an error budget analysis are presented as applied to the Aerodynamic Deorbit Experiment (ADE) CubeSat. The ADE mission will demonstrate accelerated deorbit capability from an initial geosynchronous transfer orbit (GTO) using a deployable drag sail. ADE presents a novel application of a PTE. This PTE will function at Earth rather than at Mars, flying on a small satellite with a commercial off-the-shelf (COTS) inertial measurement unit (IMU), which is in contrast to large interplanetary probes with advanced IMUs. PTE is especially useful for satellites like ADE without GPS on-board, as a GPS-produced position and time could be used to propagate and generate accurate periapsis time tables. The PTE algorithm is similar to the PTE used on Mars Odyssey and MRO, although the exact implementation of the earlier algorithms is unknown as these heritage PTEs are considered proprietary.

ADE will apply PTE to control the timing of IMU data acquisition for each drag pass centered on periapsis. This automatic periapsis estimation ability is desired to avoid the operational constraint of frequently uploading tables of periapsis times. Additionally, using daily two-line elements to propagate out these periapsis times requires assuming a certain drag sail orientation and atmospheric conditions, whereas using actual acceleration data does not require these assumptions. The PTE mathematical model is presented in Section 2, and the application of PTE to the ADE mission is provided in Section 3. Discussion of PTE simulation and testing is presented in Section 4, and analysis of error sources is given in Section 5. Conclusions are provided in Section 6.

Copyright © A. Deepak Publishing. All rights reserved.

2. Periapsis Time Estimation Mathematical Model

The PTE algorithm uses accelerometer data collected onboard the spacecraft to calculate the orbital period of previous orbits, as well as the estimated change in velocity, or ΔV, at each periapsis pass. Data from the two most recent drag passes are needed to calculate the previous orbit period and predict the time of the next periapsis. Figure 1 is a diagram and timeline representing the current orbit (red), as well as the previous orbit before the most recent drag pass (black). The times of the two most recent periapses are given by t_{i-1} and t_i, and are found by calculating the time centroids of the acceleration data gathered around those drag passes. The prior orbital period, T_{i-1}, is estimated as the difference between the two prior drag pass centroids. The time of the upcoming periapsis that is to be estimated is represented by t_{i+1}.

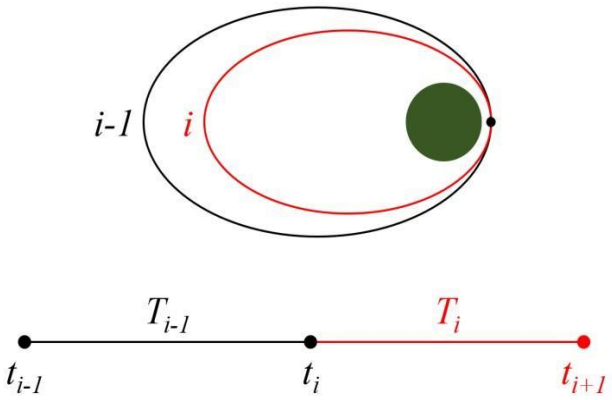

Figure 1. Orbital diagram and timeline.

Equations from two-body orbital mechanics are used to calculate the upcoming periapsis time. The following equations can all be found in Curtis's *Orbital Mechanics for Engineering Students* (2005). From the prior orbital period, the semi-major axis of the previous orbit can be found as

$$a_{i-1} = \sqrt[3]{\frac{\mu T_{i-1}^2}{4\pi^2}}. \tag{1}$$

The periapsis velocity at time t_i, without yet considering atmospheric drag, is calculated as

$$V_{i^-} = \sqrt{\mu\left(\frac{2}{r_p} - \frac{1}{a_{i-1}}\right)}. \tag{2}$$

In Eqn. 2, the radius at periapsis, r_p, is based upon the most recent orbit determination solution, which is from sources such as TLEs. Atmospheric drag is approximated as an impulsive change in velocity in the direction opposite to the spacecraft's velocity at periapsis. The magnitude of this ΔV is calculated by integrating the acceleration data obtained during the drag pass using the trapezoidal approximation method. Figure 2 depicts the discussed information of interest from an example drag pass. The change in velocity due to the drag pass, ΔV_i, is calculated as the area under the acceleration curve.

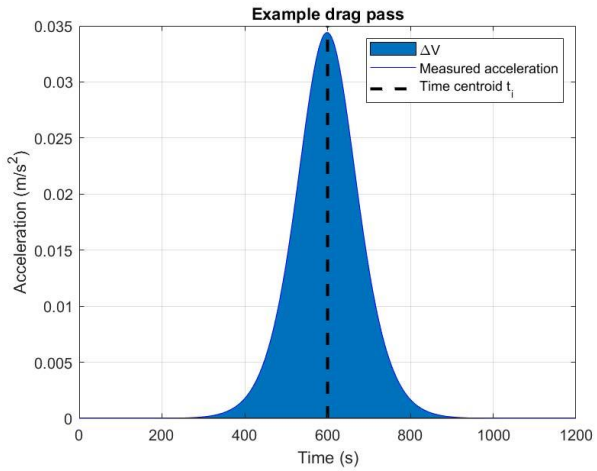

Figure 2. Sample drag pass acceleration data, time centroid, and change in velocity.

To calculate the velocity at periapsis of the current orbit including the effect of the drag pass, a simple subtraction is used: $V_{i^+} = V_{i^-} - \Delta_{i^+}$, where V_{i^+} is the velocity at periapsis after the drag pass ΔVhas been applied. The following equations, alternate forms of Eqn. 1 and Eqn. 2 respectively, can then be used to calculate the period of the current orbit, T_i. Again, the radius of periapsis is based upon the most recent orbit determination.

Copyright © A. Deepak Publishing. All rights reserved.

$$a_i = -\frac{\mu}{V_i^2 + -\frac{2\mu}{r_p}} \quad (3)$$

$$T_i = 2\pi\sqrt{\frac{a_i^3}{\mu}} \quad (4)$$

Finally, the estimated time of the next periapsis is calculated as

$$t_{i+1} = t_i + T_i. \quad (5)$$

This process allows each subsequent periapsis time to be predicted based upon the prior two periapsis centroids, and the measured acceleration pulse during the most recent drag pass.

3. PTE Application to the Aerodynamic Deorbit Experiment

3.1. Aerodynamic Deorbit Experiment Mission Overview

The Aerodynamic Deorbit Experiment (ADE) is a 1U CubeSat in development at Purdue University. Its primary purpose is to assess the performance of deployable drag sail that is designed to provide aerodynamic stability around periapsis. This device is a prototype of a drag sail design that can be used to accelerate the end-of-mission deorbit of host satellites. ADE is expected to launch in 2021 aboard a United Launch Alliance Atlas V launch vehicle. It will be deployed into a geosynchronous transfer orbit (GTO) with the parameters provided in Table 1. It is expected that ADE will receive TLE updates from the U.S. Air Force 18th Space Control Squadron approximately once per day.

Table 1. Nominal Initial Orbital Parameters

Parameter	Value
Perigee Altitude (r_p)	185 km
Apogee Altitude (r_a)	35,786 km
Eccentricity (e)	0.7306
Period (T)	10.51 hours
Inclination	27°
Argument of Periapsis	180°

The mass of the ADE CubeSat is 2.0 kg. The deployable drag sail design consists of four 1 m long booms, to which four triangular sections of drag sail material are secured, forming a square pyramid geometry (Long and Spencer, 2018; 2017; 2016).

3.2. Application of PTE

To characterize the performance of the drag sail, ADE is equipped with an inertial measurement unit (IMU) that records three-axis accelerations, angular rates, and magnetometer readings during drag passes. Due to CubeSat power limitations, only 25 minutes of IMU data acquisition is planned each orbit, centered on periapsis. With the drag sail deployed, the orbit period changes rapidly from the initial value of 10.5 hours. Control of IMU data acquisition is based upon a periapsis time table that can be updated via file uplink from ground operators, or autonomously updated through the PTE process. PTE will initially operate in a test mode, where the calculated periapsis times can be verified on the ground, but the periapsis time table is not autonomously updated. Following ground verification of proper performance, the PTE process will be commanded into operational mode, allowing autonomous updates of the periapsis time table.

3.3. IMU Characteristics

The ADE spacecraft is equipped with the UM7 IMU from Redshift Labs. The UM7 is a micro-electromechanical (MEMS) IMU with three-axis accelerometers, gyros, and a magnetometer. The UM7 datasheet provides specifications on accelerometer performance. The bias change vs. temperature in the X and Y axes is $-0.0074\ m/s^2$ and $-0.0147\ m/s^2$ in the Z axis (Redshift Labs, 2018). The drag pass acceleration magnitude is expected to be about $0.03\ m/s^2$. Therefore, with temperature ramp ups of 10 to 15 degrees, the resulting bias will likely be greater than the magnitude of the acceleration pulse during a drag pass. The datasheet does not offer information on the root-mean-square noise of the accelerometer. To experimentally estimate the noise characteristics of the IMU, static

Copyright © A. Deepak Publishing. All rights reserved.

test data were acquired in ambient and vacuum conditions. The calculated noise characteristics are summarized in Table 2.

Table 2. Experimental Noise Characteristics of IMU Found Using Test Data

IMU Axis	Root Mean Square (m/s2)
X	0.0047
Y	0.0046
Z	0.0046

From Table 2, the RMS noise in the X and Y axes is about 0.005 m/s^2 and 0.007 m/s^2 in the Z axis. Since the expected acceleration magnitude is about 0.03 m/s^2, these observed noise levels will be significant relative to the drag pass. The Z axis being noisier than the X and Y axes is supported by the bias change vs. temperature specifications in the datasheet, which shows the Z axis as more susceptible to temperature-induced bias, indicating that the X and Y axes accelerometers are less susceptible to noise and bias than the Z axis accelerometer.

As stated on the datasheet and observed through testing, temperature variations cause a bias in the data gathered within the operating temperature range provided of −40°C to 85°C (Redshift Labs, 2018). The IMU temperature increases with time following turn-on and results in a corresponding increase in acceleration, as shown in Figure 3 (left side chart). The right plot in Figure 3 depicts the correlation between measured acceleration and temperature during this static test.

3.4. IMU Data Processing

A data processing scheme will be run on the data collected from the IMU before the data are passed to the PTE algorithm. A window filter will filter out noise, and a temperature-acceleration calibration will correct for changes in accelerations due to drift over time and temperature-induce bias. To correct the accelerometer data, a cubic fit is performed on calibration acceleration and temperature data collected during the drag pass. Since the durations of the acceleration pulse during drag passes are expected to be less than the 25 minutes of IMU collection, two-and-a-half-minute calibration periods are utilized from the beginning and end of the acceleration dataset for each drag pass. These pre-and post-pass periods are characterized by negligible acceleration at orbit altitudes with negligible atmospheric density. The calibration process then subtracts out the fitted bias and drift.

Both IMU noise and bias pose an issue to the PTE, as non-zero noise and bias artifacts after correction will be integrated in calculating the estimated ΔV each

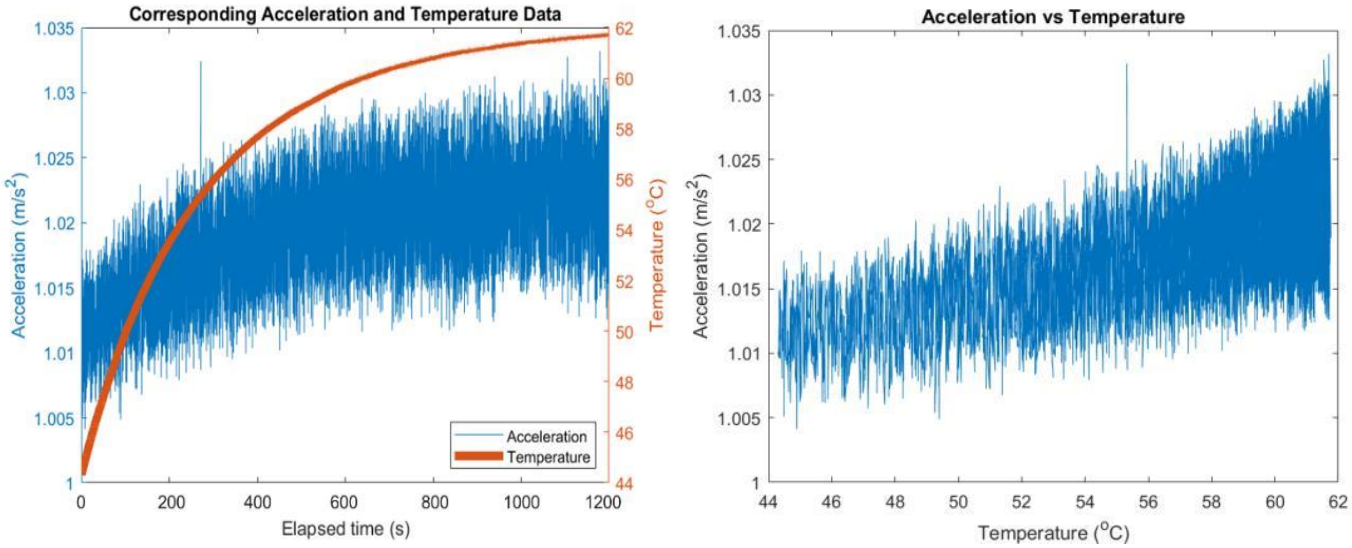

Figure 3. Example of temperature-induced acceleration bias.

Copyright © A. Deepak Publishing. All rights reserved.

pass, incorrectly increasing or decreasing the ΔV. To mitigate this issue, a thresholding function was implemented to allow PTE to discard acceleration data below the filtered data's noise levels, which also discards some remaining bias. The threshold has been chosen to be a quarter of the peak of the pass, updating with each pass.

4. PTE Simulation and Testing

High fidelity propagation software was used to test the functionality and accuracy of the PTE. An ADE scenario was created in the General Mission Analysis Tool (GMAT) with an epoch chosen to be June 1st, 2021. The scenario was run until deorbit, and simulated acceleration data was calculated from the GMAT data. Acceleration due to atmospheric drag is input into PTE at one-second timesteps, providing a set of nominal accelerometer data for every drag pass. The acceleration due to lift and side force are assumed to be zero so that all acceleration measured by the simulated IMU is assumed to be drag. Random noise is added to the acceleration data points by using the values in Table 2 as standard deviations for a Gaussian distribution. The biased acceleration data and the temperature time-series data are simulated using two-term exponential functions based on curve-fit parameters gathered from static testing data. These data include the temperature ramp-up that results in observed acceleration bias, different from the noise parameters in Table 2, which were measured after temperature stabilization. Each bias parameter is allowed to deviate in a Gaussian distribution centered around the original curve-fit parameters, resulting in randomly generated but correlated curves. The standard deviations used for these Gaussian distributions were derived from coefficient 95% confidence intervals calculated during the two-term exponential curve fit.

After the propagator generates the drag profile data and the noise and bias are applied, both PTE and its data processing scheme are run, utilizing the flight-like data for end-to-end testing of the PTE algorithm. The radius of periapsis that is input into PTE is held constant as the initial radius of periapsis. This testing provides the basis for the error analysis presented in Section 5.

5. Error Analysis

For the ADE application, PTE is used to schedule the timing of IMU data acquisition, so that acceleration and angular rate data from drag passes can be used to assess the aerodynamic stability provided by the drag sail. Periapsis time predictions resulting from the PTE process must be accurate enough to ensure that the drag pulse is captured during the central 20 minutes of the 25-minute IMU data collection period. This section will discuss the error sources in the PTE algorithm and their impact on the accuracy of the periapsis time estimation. Error sources are compared against high fidelity simulator data. The mean and standard deviation of the error due to each source is computed. These statistics are calculated for the beginning 25% of the mission's periapsis passes, the middle 50%, and the end 25%, and are summarized in Section 5.6.

The magnitude of the periapsis timing error is heavily dependent on the size of the current orbit. Orbits with a higher apoapsis see exponentially larger errors in periapsis time estimation for a constant error in ΔV. Early in the ADE mission, the highly elliptical geosynchronous transfer orbit will cause PTE to be prone to large periapsis time errors. However, as the orbit's apoapsis decreases, the PTE error will decrease. Figure 4 demonstrates the relationship between apoapsis altitude and periapsis time error for a set of errors in calculating ΔV from an acceleration profile. Periapsis altitude was held constant at 185 km.

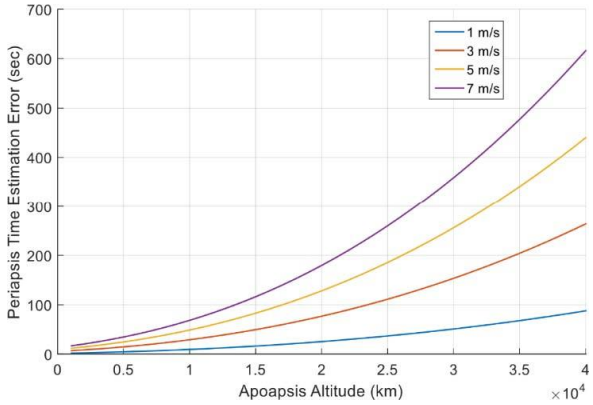

Figure 4. PTE time error vs. apoapsis altitude for given errors in estimated ΔV.

Copyright © A. Deepak Publishing. All rights reserved.

Since PTE must operate on flight computers with limited processing power, the algorithm was created to be as computationally simple as possible. Several simplifying assumptions were made to streamline the algorithm and reduce the computational load; however, the simplifications introduce error sources that impact the accuracy of periapsis time estimation. Assumptions include that the cumulative change in velocity during a drag pass is treated as an impulsive ΔV occurring at periapsis. Additionally, the periapsis altitude is held constant as from the most recent orbit state update uplinked from ground operators. Finally, timing calculations are based upon two-body orbital mechanics, neglecting third-body effects and non-gravitational perturbations. Each of these assumptions is analyzed to determine the contribution to the PTE error budget.

5.1. Impulsive Velocity Change Assumption

To simplify calculations, PTE approximates the change in velocity due to the drag pass as an impulsive ΔV applied at periapsis. However, treating the distributed change in velocity as an instantaneous ΔV creates a source of error. To characterize the magnitude of this error, an ADE scenario was created in the General Mission Analysis Tool (GMAT). The ΔV was calculated for each drag pass and given to both PTE and GMAT for calculation of the next orbit period so that the same amount of drag would be applied in each propagator. Both PTE and GMAT used the same initial orbit, but differed in treating the ΔV as impulsive or finite, respectively. To isolate the error due to the impulsive ΔV assumption, the GMAT scenario was simplified to match PTE as much as possible. In GMAT, the spacecraft was given a drag coefficient of 0 to remove atmospheric effects, since the finite maneuver represents the atmospheric drag pulse. The GMAT propagator was chosen to be two-body, so each propagator used simple two-body mechanics. The finite maneuver in GMAT was implemented by targeting the desired periapsis velocity after the pass, given a mean pass duration of 800 seconds and allowing the thrust efficiency to vary to achieve the specific ΔV. The period output by GMAT was substituted into PTE for each pass, and the difference in error between the two methods was taken to be the error due to the impulsive velocity assumption. The error over the mission lifetime is shown in Figure 5. The error statistics are summarized in Table 3.

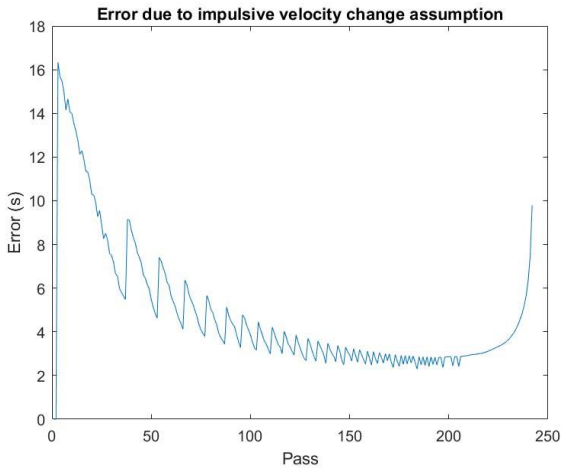

Figure 5. Time error due to impulsive velocity assumption.

The error due to the impulsive velocity assumption decreases throughout the course of the mission, corresponding with the shrinking radius of apoapsis, as discussed in Figure 4.

5.2. Constant Periapsis Altitude Assumption

PTE uses the orbital periapsis radius in its calculations twice per iteration. The radius of periapsis is first used in Eqn. 2 to calculate the initial velocity at periapsis, and then in Eqn. 3 to estimate the post-pass semi-major axis. The radius of periapsis is the only term in PTE's calculations that cannot be estimated using IMU data, and therefore must be updated from ground operators as it changes throughout the mission. Figure 6 shows the relationship between the error in periapsis radius and PTE time error for several orbits of different apoapsis altitudes. The ΔV of the drag pass also impacts this error, such that larger values of ΔV lead to higher time error. A 6 m/s velocity change was used to generate the data in this figure.

The ADE mission will receive updates to its orbit parameters from the 18th Space Control Squadron approximately once per day, and as such, the radius of periapsis is assumed to be constant throughout each

Copyright © A. Deepak Publishing. All rights reserved.

Table 3. ADE Periapsis Time Estimation Error Budget

	Beginning 25% of Deorbit		Middle 50% of Deorbit		Final 25% of Deorbit	
Error Source	Mean Error (s)	Standard Deviation (s)	Mean Error (s)	Standard Deviation (s)	Mean Error (s)	Standard Deviation (s)
Constant Periapsis Radius Assumption	0.6	0.1	0.3	0.04	0.1	0.05
Impulsive Velocity Assumption	8.7	3.6	3.6	0.9	3.4	1.2
Two-Body Orbit Assumption	20.8	8.3	4.8	3.1	0.5	6.6
IMU Noise	2.5	5.6	1.1	3.6	0.4	3.5
IMU Bias	17.5	21.5	10.9	9.1	9.5	6.2
Drag Centroid Offset from Periapsis	0.0	0.3	0.0	0.4	0.0	0.5
Threshold Function	27.7	9.8	9.5	3.4	6.2	3.7
Non-Drag Acceleration	44.8	15.6	16.0	5.4	10.2	2.6
Total	122.6	30.2	46.2	12.1	30.3	10.8

day before update, causing some error in PTE's calculations. Based on deorbit rate analyses done using GMAT, the mean daily change in periapsis radius as it oscillates throughout an orbit is estimated to be 7.4 km towards approximately the last 25% of the mission with a standard deviation of 2.1 km, while for the beginning 25% and middle 50% of the mission, the mean daily change is about 3.8 km and 4.5 km, both with standard deviations of 0.6 km. Using Figure 6 early in the ADE mission, while the apoapsis altitude lies near 35,000 km, this would result in a mean 0.6 sec error in periapsis time. The other results of transforming periapsis radius error into PTE error are summarized in Section 5.6. As with most error sources, this time error will decrease as ADE deorbits and the radius of apoapsis decreases, even with a greater daily change in radius of periapsis. Over the deorbit timeline, the PTE error due to a changing periapsis radius is negligible in comparison with the other error sources.

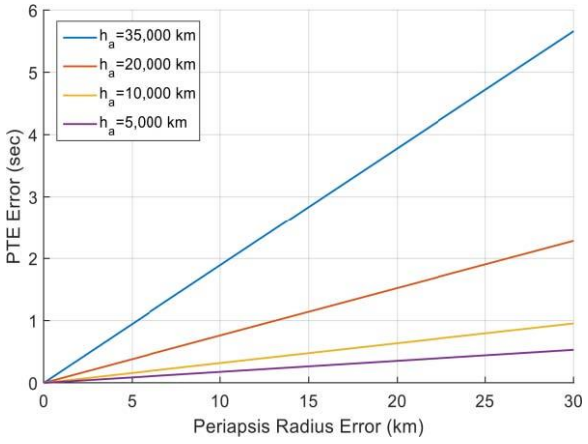

Figure 6. PTE time error vs. periapsis radius error for given apoapsis altitudes.

5.3. Two-Body System Assumption

As previously stated, PTE assumes that ADE operates within a two-body system with the Earth as the primary body, ignoring the effects of the Moon, Sun, and other perturbations. To analyze the error due to this assumption, results from PTE were compared with results from GMAT. For each run of PTE, the PTE-calculated ΔV was applied as an impulsive maneuver in the anti-velocity direction in GMAT using the same initial pass orbit. GMAT propagated to the next periapsis and returned the orbit period.

Figure 7 compares the resulting periods calculated within PTE using the two-body assumption and using the GMAT 3-body propagator with a JGM-3 4th order gravity model. Over the deorbit timeline of ADE, PTE's two-body assumption gives less accurate results than GMAT. Initially, PTE's calculated orbit period is around two to three minutes longer than GMAT's propagated orbit period. This would indicate that third-body effects and other perturbations may decay the orbit more significantly than PTE expects; these effects are dependent on the initial orbit geometry and actual epoch, which will not be known exactly until launch. However, as the radius of apoapsis shrinks along with perturbations outside of the two-body assumption, PTE's calculations become more accurate and the error decreases. The error in Figure 7 is the

Copyright © A. Deepak Publishing. All rights reserved.

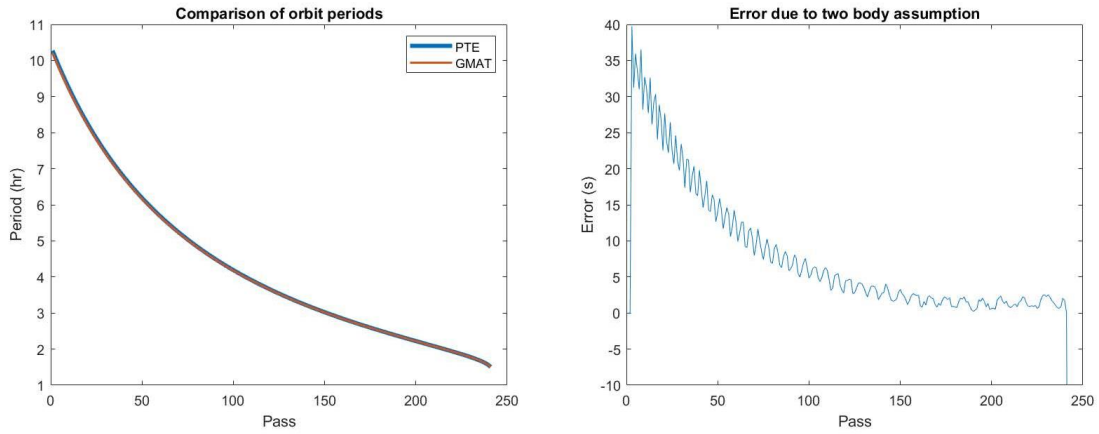

Figure 7. Comparison of predicted orbit periods from PTE calculations and GMAT.

contribution of the two-body assumption to the error within PTE rather than the difference in periods, and is calculated by comparing GMAT data with PTE data.

5.4. IMU Error Sources

Other sources of error within the results of the PTE stem from drift and calibration issues with the IMU used to measure acceleration. IMU accelerometer data error can be characterized as noise, drift, and temperature-induced bias.

5.4.1. IMU Noise

The IMU per-axis RMS noise, as summarized in Table 2, translates to 0.0098 m/s^2 in 3-axis magnitude. To filter out this noise, a window filter has been implemented. A window filter processes data by replacing each individual data point with the average of all data points within the defined window centered on the individual point. The first and last half-windows of data points are not processed, because the window would fall outside of the data set. Instead, the values in these unfiltered ranges are respectively set equal to the first and last filtered value.

For PTE, the window size is defined as 120 data points to capture two minutes of data. Figure 8 shows an example unbiased drag pass with simulated noise overlaid with the same the same drag pass after the window filter has been applied. Figure 8 shows that although the noise magnitude is large in comparison to the drag pass, a noise filter can be effective in determining the acceleration signal, with a small amount of residual error.

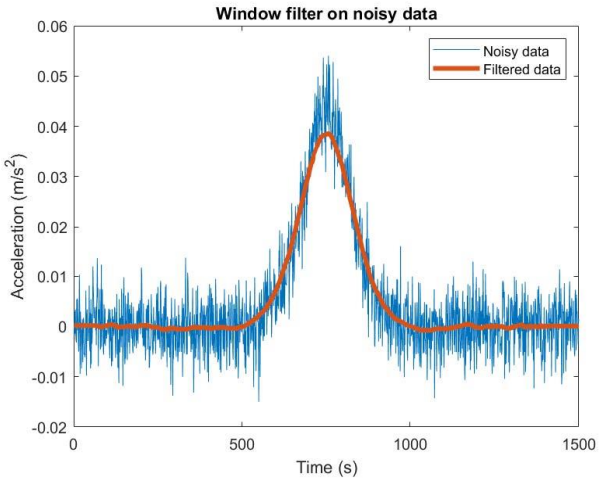

Figure 8. Comparison of unbiased pass data before and after noise filter.

5.4.2. IMU Drift and Bias

Due to temperature ramp up from internal heat generation as the IMU is powered on at the beginning of each pass, the IMU experiences a temperature-dependent bias as well as a time-dependent drift, which will be corrected using the calibrated accelerometer data from the beginning and ending 150 sec of the 25 min dataset. Figure 9 shows this correction performed

Copyright © A. Deepak Publishing. All rights reserved.

on a simulated biased drag pass. It can be seen in Figure 9 that the temperature-based correction can significantly decrease the bias using the correlation between the observed bias and the temperature ramp up.

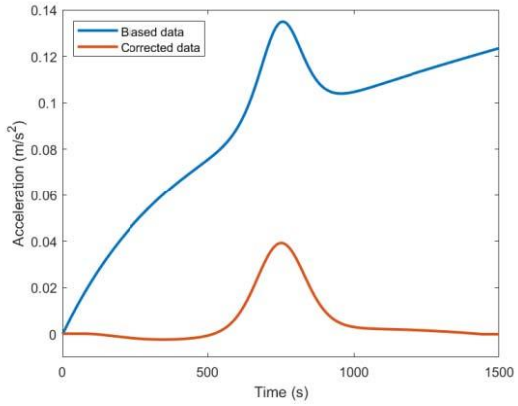

Figure 9. An example biased pass after bias correction.

To isolate the error due to the IMU noise and bias, the overall PTE error over the mission timeline was calculated in the propagator twice, once with only simulated noise and once with only simulated bias. Figure 10 shows these error results. The error without noise or bias curve represents the inherent error due to the thresholding function, discussed in the upcoming section. This threshold error is the base error onto which the noise and bias errors are added in this situation. Therefore, the error of note is the deviation between the threshold error and the noise and bias errors, and is not relative to the zero-error line.

5.4.3. Threshold Function

PTE incorporates a minimum acceleration threshold within its calculations to avoid integrating noise and bias artifacts. Implementation of this threshold reduces the computed drag pass duration, and therefore results in an underestimate of the velocity change during a drag pass. Through testing of different thresholds, it was found that higher thresholds resulted in far better performance. Although higher thresholds can underestimate the ΔV, lower threshold settings can result in noise or bias artifacts being included in the ΔV calculation, resulting in large PTE errors. The benefit of a threshold is shown in Figure 11, where the error over the mission has been calculated with and without a threshold. It can be seen that a threshold can significantly decrease the magnitude of error.

However, PTE has an inherent error due to the threshold function. To approximate this error, the difference in overall error in PTE with and without the threshold was calculated in the propagator without noise or bias, shown in Figure 12 below. Despite this error, the threshold function must be implemented, as it is necessary for avoiding greater error caused by noise and bias.

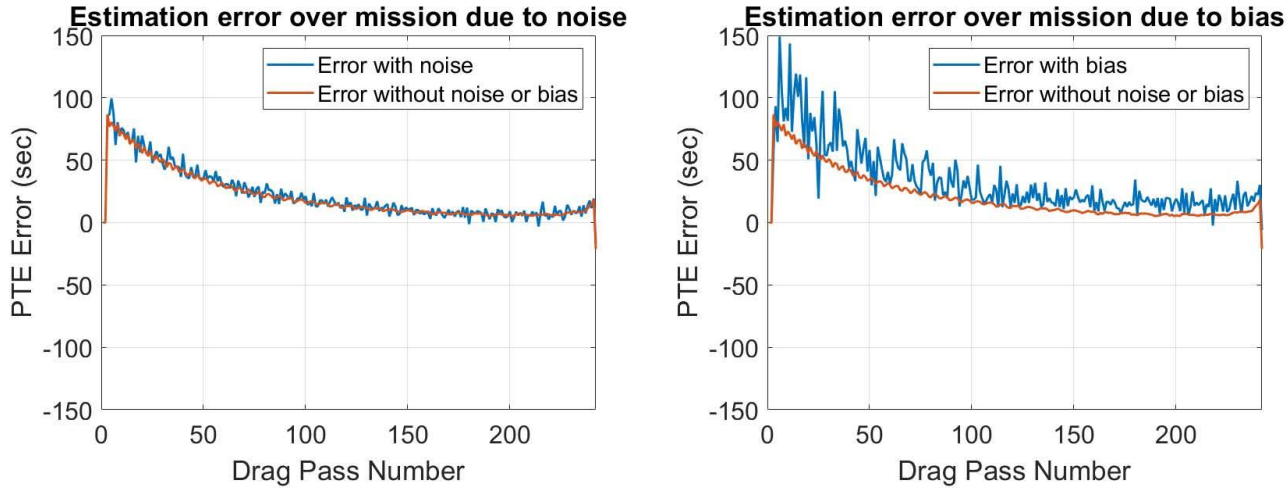

Figure 10. PTE Threshold Function.

Copyright © A. Deepak Publishing. All rights reserved.

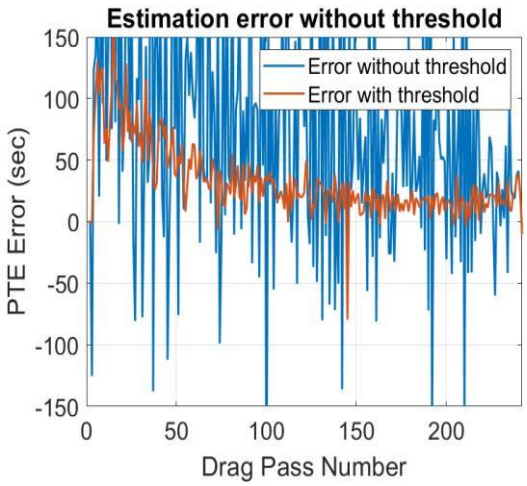

Figure 11. Error in PTE with and without a threshold.

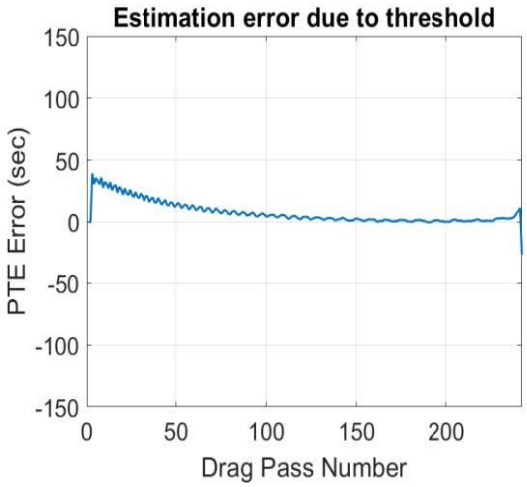

Figure 12. Base error in PTE without noise or bias.

5.5. Additional Error Sources

Other sources outside of the scope of assumptions or hardware limitations remain. These error sources include the effects of uneven atmospheric density profiles resulting in asymmetric acceleration profiles, and the effect of any lift forces being included in the measured acceleration profile.

5.5.1. Drag Centroid Not Equivalent to Periapsis

PTE assumes that the time centroid of each drag pass is the true periapsis of each pass. However, it is likely that this is not the case for every drag pass, due to the local atmosphere. The actual Earth atmosphere is inconsistent compared to the Earth GRAM-generated atmosphere, and as such, actual drag passes will not be symmetrical, bellcurve-like passes but rather more jagged and uneven. The centroiding method of the PTE is similar to a weighted average in that each time step is weighted by its corresponding acceleration. Thus, for rough pass curves, the centroid may be pulled towards a time that is not the true periapsis.

To investigate the effect of this on PTE, aerobraking data from Mars Reconnaissance Orbiter (MRO) were analyzed using PTE's centroiding scheme. Orbits 280 and 211 were chosen for comparison, as orbit 280 has a jagged profile due to a spike of double density, as described by Tolson, and orbit 211 has a typical, nearly symmetrical profile (Tolson, 2011). The acceleration aerobraking data do not mark periapsis, but the reconstructed density data record time from periapsis; using this, the density data were overlaid and scaled to estimate the pass periapsis.

As shown in the right side plot in Figure 13, PTE is fairly accurate when centroiding periapses of typical passes. In this case, with orbit 211, the calculated centroid of the acceleration pulse is within 15 seconds of the periapsis time reconstructed from the navigation data. However, the left graph of orbit 280 shows a more complex case of an inconsistent density profile. Around 120 to 180 seconds, atmospheric density roughly doubles in magnitude and fluctuates until the peak at around 280 seconds. Since PTE uses a centroiding scheme similar to a weighted average, PTE is prone to shift the centroid towards areas of higher density. With this rough profile, the PTE error in calculating the centroid of the acceleration pulse is about 45 seconds. Although MRO's spacecraft, orbit, and planetary atmosphere are different from ADE's, the underlying mechanism for centroiding drag passes are similar, and thus will have a similar error. To further analyze the error due to inconsistent atmospheres, a Monte Carlo simulation was created in MATLAB. This simulation uses the data from passes 5, 120, and 200 to represent the beginning, middle, and end of the mission, taking the velocity data and density profile. The Monte Carlo simulation divides up the density profile into sections of length 5 minutes, 4 minutes, 3 minutes, 2 minutes, 1 minute, 30 seconds, 15 seconds,

Copyright © A. Deepak Publishing. All rights reserved.

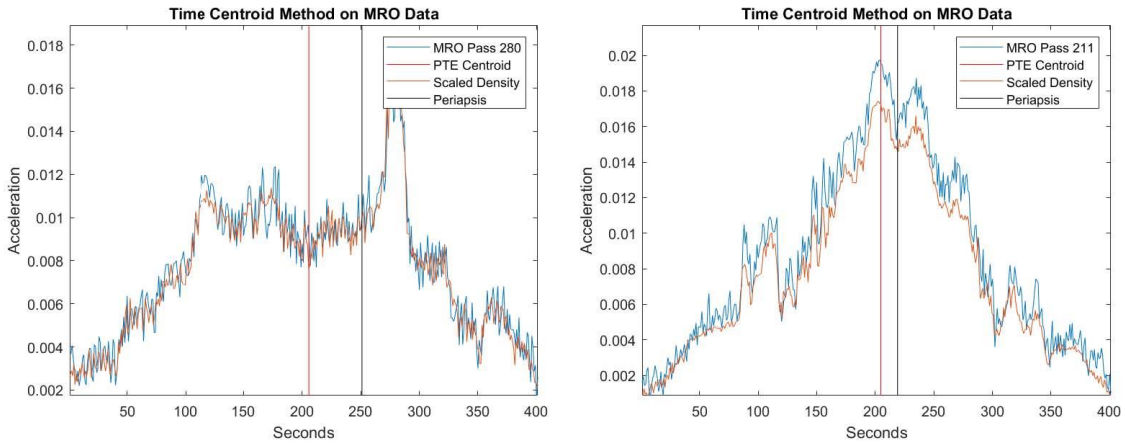

Figure 13. PTE centroided periapsis run on MRO aerobraking pass data compared to actual periapsis.

and 5 seconds. Then, for each section length, the simulation runs through each section of the drag pass individually, allowing the density in that section to deviate normally. From EarthGRAM 2016, the 1-sigma deviation of density at 185 km is around 10%, which is used in this simulation. The acceleration profile is calculated using each perturbed density profile as usual, and PTE's centroiding scheme is run to collect the time centroid. This process runs for each section length 1000 times. Finally, the mean and standard deviation of the difference between the time centroids and the true periapsis are calculated. All values are contained in Table 3. The mean and standard deviation for each time period are very small. This indicates that, although the error may be significant for a single pass, over the course of the mission these errors will average out to have a negligible overall effect on the accuracy of PTE.

5.5.2. Acceleration from Lift Vectors in IMU Data

Since the orientation of the spacecraft cannot be known, all acceleration measured by the IMU is assumed to be drag. Extracting the acceleration solely due to drag would require knowledge of absolute attitude, which ADE does not possess. However, certain orientations of the spacecraft could cause lift to be produced. Within PTE, the fraction of the overall acceleration that results from lift causes an overestimation of the drag produced. For ADE, the square pyramid drag-sail geometry provides passive aerodynamic stability near periapsis about the maximum drag orientation (Black, 2020). As shown in Figure 14, the total angle of attack of the vehicle is below 10 deg near periapsis. For these low total angles of attack near periapsis, drag is dominant over lift, and the vehicle L/D is < 0.2.

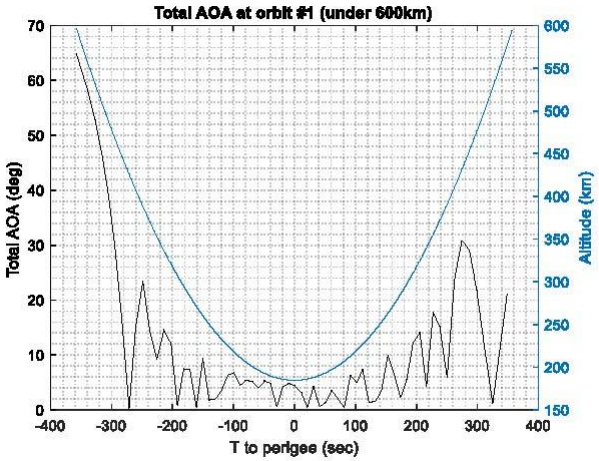

Figure 14. Total angle-of-attack and altitude vs. time to perigee.

Other non-drag sources of acceleration can include gravity gradients and SRP along with the more significant sources of bias and vibration (Jah, 2001). The material for the drag sail has been chosen to be transparent to avoid SRP effects. Analysis has shown SRP- and gravity gradient-induced accelerations to be negligible during drag passes due to the periapsis altitude.

Copyright © A. Deepak Publishing. All rights reserved.

Bias and vibration in the acceleration data are filtered out of the processed data, as discussed previously. To analyze the effect of lift as a source of acceleration, the maximum L/D ratio of 0.2 was used to subtract lift from the ΔV calculated by PTE in each pass. The difference between the estimated periapsis times was taken to be the error of assuming all acceleration is drag. Since this is the maximum lift case, it is an overestimate for this error but still provides insight on trends and relative magnitude. The error due to lift is large during the beginning of the mission, but decreases significantly over time with decreasing radius of apoapsis. The error statistics are summarized in Table 3.

5.6. Periapsis Time Estimation Error Budget

In summary, the primary causes of error in periapsis time estimation are the impulsive velocity assumption, the two-body system assumption, the IMU noise and bias, and lift acceleration. Errors due to the constant periapsis radius assumption and atmospheric inconsistencies are much smaller than the other error sources. The mean and 1-sigma errors from the identified sources are summarized in Table 3. These errors are actual and can be positive or negative. Errors are provided for the beginning, middle, and end of the ADE deorbit profile.

The total standard deviations for each phase in Table 3 are calculated as the Root Sum Squared totals. The total mean error over the entire mission timeline is estimated to be 61.3 seconds, or approximately a minute, and the estimated mean 1-sigma error over the mission is 16.3 seconds. As the mission progresses, the mean error tends to decrease significantly; however, when rapid deorbit begins to occur at the very end of the mission, the variation in error will increase due to much larger atmospheric density and drag. Overall, since the drag pass durations are expected to be around 15 minutes, these errors will fall within the requirements that the PTE algorithm is sufficiently accurate to acquire the drag pass data within a 25-minute data collection period (less 150 seconds at the beginning and the end of the data acquisition period for accelerometer calibration).

5.7. Cumulative High-Fidelity Simulation

Since the estimated error budget in Table 3 is calculated from individual error sources, a final analysis of PTE's accuracy was completed to compare the overall error with the budget in Table 3. High fidelity data was generated in GMAT with a three-body propagator, JGM-3 4th degree gravity model, and atmospheric drag and input into PTE. Figure 15 shows the plotted error over the mission timeline. Table 4 summarizes the statistics in the same format at Table 3 for comparison with the results of Table 3 in the final row. Note that the GMAT data uses a spherical drag model and as such the error due to the drag assumption discussed in Section 5.5.2 does not carry over into the final comparison in the last row.

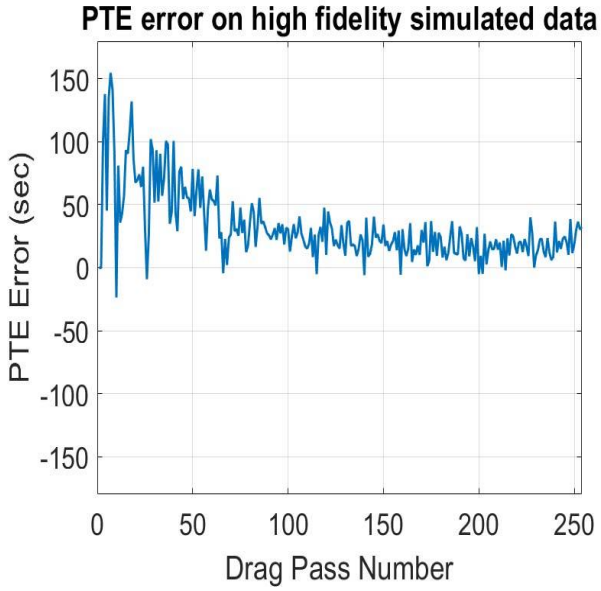

Figure 15. PTE error over mission timeline on high fidelity data.

Table 4 shows that the error budget estimated in Table 3 is close to the error calculated in a high-fidelity run. The exact magnitude of error will change between runs due to the random error and temperature bias and will differ during the actual mission due to different initial orbit conditions. However, overall, the results from the high-fidelity data support the relative magnitudes reached through this error analysis.

Copyright © A. Deepak Publishing. All rights reserved.

Table 4. Cumulative Error Comparison with Error Budget

	Beginning 25% of Deorbit		Middle 50% of Deorbit		Final 25% of Deorbit	
	Mean Error (s)	Standard Deviation (s)	Mean Error (s)	Standard Deviation (s)	Mean Error (s)	Standard Deviation (s)
Total	66.5	36.0	24.4	13.3	17.4	10.3
Individual Combined (Non-Drag Excluded)	77.8	25.9	30.2	10.9	20.1	10.5

6. Conclusions

Periapsis time estimation is a technique for using on-orbit accelerometer data from drag passes to update predicted times of future periapses. For the ADE mission, the PTE process is required in order to capture IMU data during drag passes, which will then be used to characterize the aerodynamic stability provided by the drag sail.

The accuracy of the PTE algorithm is largely driven by the assumptions of impulsive velocity and a two-body system within the algorithm. Other error sources external to PTE include the IMU noise, drift, and temperature bias. Use of an IMU more accurate than the MEMS UM7 would allow improved PTE performance. A rigorous analysis of the error sources in the PTE algorithm indicate that the PTE error is greatest in the early portion of the ADE deorbit timeline, when the orbit eccentricity is the greatest. Mean PTE errors of 123 sec with standard deviation of 30 sec are expected during the early part of the mission. As the vehicle deorbits, PTE accuracy improves, reaching a mean error of 46 sec with a 12-sec standard deviation prior to reentry. During the end of mission, mean error decreases to 30 sec with a standard deviation of 11 sec. The approach presented for assessing the accuracy of the PTE algorithm also has applications to planetary aerobraking, as well as science missions that involve repeated dips into a planetary atmosphere.

Acknowledgements

The following people are acknowledged for their contribution to IMU testing: Ben Hilker, Maaninee Gupta, and Dhruv Mathur. Thank you to Sebastian Tamrazian for DMSC analysis of ADE, which produced results used in PTE simulation and testing. The Space Flight Projects Laboratory is acknowledged as well, for their support of PTE and the ADE mission.

References

Black, A. and Spencer, D. A. (2020): DragSail Systems for Satellite Deorbit and Targeted Reentry. *J. of Space Saf. Eng.*, pre-print. doi:10.1016/j.jsse.2020.07.030.

Denis, M. et al. (2018): Thousand Times through the Atmosphere of Mars: Aerobraking the ExoMars Trace Gas Orbiter, presented at SpaceOps Conf., Marseille, France, May 28–June 1. Paper AIAA 2018-2713. doi:10.2514/6.2018-2713.

Carrelli, D. et al. (2012): Autonomous Aerobraking for Low-Cost Interplanetary Missions. *Acta Astronautica*, Vol. 93, pp. 467–474.

Chapel, J. D. et al. (2005): Aerodynamic Safing Approaching for the 2001 Mars Odyssey Spacecraft During Aerobraking. *J. Spacecr. Rockets*, Vol. 42 (3), pp. 416–422.

Curtis, H. (2005): *Orbital Mechanics for Engineering Students*. Burlington, MA: Elsevier.

Hanna, J. L. (2002): Approaches to Autonomous Aerobraking at Mars, Masters Thesis, School of Engineering and Applied Science, The George Washington University, Washington, DC

Jah, M. K. (2001): A Proposed Use of Accelerometer Data for Autonomous Aerobraking at Mars, presented at the AAS/AIAA Astrodynamics Specialist Conf., Quebec City, Quebec, CA, July 30–August 2. Paper AAS 01-386.

Jah, M. K. et al. (2008): Mars Aerobraking Spacecraft State Estimation by Processing Inertial Measurement Unit Data. *J. Guid., Control, Dyn.*, Vol. 31 (6), pp. 1802–1826.

Copyright © A. Deepak Publishing. All rights reserved.

Jesick, M. et al. (2016): MAVEN Navigation Overview, presented at the AAS/AIAA Space Flight Mechanics Meeting, Napa, CA, February 14–18. Paper AAS 16-237.

Johnson, M. and Willcockson, W. (2003): Mars Odyssey Aerobraking: The First Step Towards Autonomous Aerobraking Operations, presented at the IEEE Aerospace Conf., Big Sky, MT, March 8–15. Paper 1169. doi:10.1109/AERO.2003.1235536.

Long, A. C. and Spencer, D. A. (2016): Stability for a Deployable Drag Device for Small Satellite Deorbit, presented at the AAS/AIAA Astrodynamics Specialist Conf., Long Beach, CA, September 12–15. Paper AIAA 2016–5676. doi:10.2514/6.2016-5676.

Long, A. C. and Spencer, D. A. (2017): A Passively Stable Pyramid Sail for the Deorbit of Small Satellite Constellations, presented at the 68th International Astronautical Congress, Adelaide, Australia, September 25–29. Paper IAC-17-A6.5.2.

Long, A. C. and Spencer, D. A. (2018): A Scalable Drag Sail for the Deorbit of Small Satellites. *J. of Small Satellites (JoSS)*, Vol. 7 (3), pp. 773–788.

Lyons, D. T. (2001): Aerobraking Automation Options, presented at the AAS/AIAA Astrodynamics Specialist Conf., Quebec City, Quebec, Canada, July 30–August 2. Paper AAS 01–385.

Maddock, R. W. et al. (2011): Implementation and Simulation Results Using Autonomous Aerobraking Development Software, presented at the AAS/AIAA Astrodynamics Specialist Conf., Girdwood, AK, July 31–August 4. Paper AAS 11-476.

Prince, J. L. H. et al. (2012): Autonomous Aerobraking: A Design, Development, and Feasibility Study. *Adv. Astronaut. Sci.*, Vol. 142. pp. 475–481.

Redshift Labs. (2018): UM7-LT Orientation Sensor. Available at: https://redshiftlabs.com.au/wp-content/uploads/2018/02/um7_datasheet_v1-6_10.1.2016.pdf (accessed September 10, 2020).

Spencer, D. A. and Tolson, R. H. (2007): Aerobraking Cost and Risk Decisions. *J. Spacecr. Rockets*, Vol. 44 (6), pp. 1285–1293.

Tolson, R. H. and Huber, L. F. (2010): Mars Reconnaissance Orbiter Accelerometer Data Archive, MRO-M-ACCEL-2-ACCELDATA-V1.0 and MRO-M-ACCEL-5-PROFILE-V1.0. Available at: https://atmos.nmsu.edu/data_and_services/atmospheres_data/MARS/mro_aerobraking.html (accessed September 10, 2020).

Tolson, R. H. and Prince, J. L. H. (2011): Onboard Atmospheric Modeling and Prediction for Autonomous Aerobraking Missions, presented at the AAS/AIAA Astrodynamics Specialist Conf., Girdwood, AK, July 31–August 4. Paper AAS 11–477.

Copyright © A. Deepak Publishing. All rights reserved.